Rolling Bearing Failure Detection in Induction Motors using Stator Current, Vibration and Stray Flux Analysis Techniques

Bessous Noureddine, Remus Pusca, R. Romary, Sbaa Salim

Rolling Bearing Failure Detection in Induction Motors using Stator Current, Vibration and Stray Flux Analysis Techniques

Bessous Noureddine
Department of Electrical Engineering, Fac. Technology
University of El Oued
El Oued, Algeria
nbessous@yahoo.fr

Pusca Remus
Laboratory of Electrotechnical and Environmental Systems
(EA-4025), Béthune, France
Univ. Artois, EA 4025 LSEE, F-62400, Béthune, France
remus.pusca@univ-artois.fr

Romary Raphael
Laboratory of Electrotechnical and Environmental Systems
(EA-4025), Béthune, France
Univ. Artois, EA 4025 LSEE, F-62400, Béthune, France
raphael.romary@univ-artois.fr

Sbaa Salim
Department of Electrical Engineering, Fac. Technology
University of Biskra
Biskra, Algeria
s_sbaa@yahoo.fr

***Abstract*—Many industrial applications use the induction machine for its advantages, like robustness. But like any other machines, it can be affected by several faults such as broken rotor bars, stator inter-turn short-circuit, bearing faults, etc. On the one hand, mechanical faults produce vibration, eccentricity and torque oscillations which influence the stator current and the distribution of the magnetic field. Therefore, early detection of mechanical faults leads to avoid damage or sudden stop of the induction machine. In this context, this paper studies the performances of three fault detection and diagnostic techniques for rolling bearing failures. The first technique is based on the stator current analysis, the second one uses the vibration signal analysis and the last technique is devoted to the stray flux signature.**

The aim of the study is to highlight the performances of stray-flux technique in the detection of inner raceway fault comparatively to current and vibration. For this study, experimental tests are realized on a laboratory test bench allowing creation of artificial bearing damage. The analysis is focused on specific harmonics related to the electrical and mechanical frequencies.

Keywords— induction motors; rolling element bearing faults; motor current signature analysis; motor vibration signature analysis; stray flux signature analysis.

I. INTRODUCTION

Induction Motors (IMs) are widely used in many industrial applications but like all electrical machines they are susceptible to many kinds of faults and their monitoring is a crucial phase to avoid the sudden stop. Generally, the fault classifications in IMs are stator faults, rotor faults, bearing faults and other faults. The fault distributions in the IMs show that bearing fault are the most likely to occur with a significant percentage which can reach 41% of the whole faults [1]. This fault produces some symptom like air-gap variation, torque oscillation, overcurrent of the stator current, excessive heating, increased losses, etc. [2,3]. In addition, Rolling Element Bearing (REB) is one of the most used types of bearings in Rotating Electrical Machines (REMs).

As the REB faults represents more than 41% of IMs faults, they are considered as major risks that can cause catastrophic damage in rotating electrical machines. So early detection of REB faults is an essential step to avoid several issues as the economic losses. Therefore they require special monitoring.

It's also known that the REB faults of IM lead to rotor eccentricity faults [4,5] because it generates airgap variation. The aim of this paper is to study the performances, the advantage and drawback of fault detection using three techniques based on the stator current, vibration signal analysis, and stray flux.

Fast Fourier Transform (FFT) is one of many tools with good efficiency for analysis of stationary operating condition. Researchers have recently used this tool to analyze signals such as the vibration signal, the stator current signal, the electromagnetic torque signal, the magnetic field signal, etc.[6-8]. The development of signal processing software opens the door to fault detection in the monitoring of REMs. The techniques as wavelet transform, Artificial Neural Network (ANN), fuzzy logic, Hilbert Transform, Empirical Mode Decomposition (EMD), Motor Vibration Signature Analysis (MVSA), Motor Current Signature Analysis (MCSA), etc. have been used to detect several faults [9-11].

Stray Flux Signature Analysis (SFSA) technique is recently attracts the attention of many researchers in REM diagnosis [12-14]. MCSA-FFT and MVSA techniques are nowadays widely used in several industrial sectors for REMs fault detection [15-18].

This paper analyses the possibility to use the stray flux for detection of the REB fault in IM and display the efficiency of this technique compared to existing ones. The sensitive frequencies relative to bearing failure are highlight for the REB fault of each technique.

The experimental results presented in this paper are obtained on a 50Hz, 4kW two-pole induction motor with artificial bearing damage The number of rotor bar is N_{rb}=28. Figure 1 shows the test bench with an IM, and a permanent magnet synchronous generator connected to a resistor used as a load to obtain different working conditions and equipment for data acquisition.

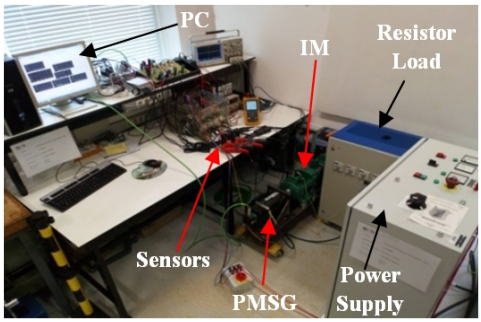

Fig. 1. Test bench used for detection of REB fault in IM.

II. REB CHARACTERISTIC FOR EXPERIMENTAL TEST

To better describe the failure which can appear in the REB, the four elements which are part of it are presented in Fig. 2. According to these parts, we can define four REB faults as follow:

1- Outer Race Fault (ORF);
2- Inner Raceway Fault (IRF);
3- Cage Fault (CF);
4- Ball Fault (BF).

The REB type used in the tested IM belongs to a 6206 series. It contains N_b=9number of balls with a diameter D_b=9.5 mm (it varies according to the manufacturer). The standard dimensions of REB 6206 are the outer diameter D_o=62mm, the inner diameter D_i=30mm, and the thickness value D_{th}=16mm.

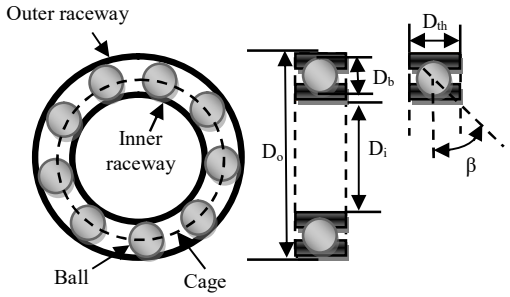

Fig. 2. Schematic description of ball bearing parts.

For the experimental tests it has been artificially prepared the **I**nner **R**aceway **F**ault (IRF) to analyze the different influences on IM behaviour. Fig. 3 shows pictures of healthy and faulty **I**nner **R**aceway (IR).


Fig.3. Picture of healthy and artificial inner raceway fault

Generally, the characteristic frequencies f_c in the spectrum of the vibration signal are given according to each element by the following formulas [19, 20]:

Outer raceway:

$$f_c = f_{OR} = \frac{N_b}{2} f_r \left(1 - \frac{D_b}{D_c} \cos \beta\right) \quad (1)$$

Inner raceway:

$$f_c = f_{IR} = \frac{N_b}{2} f_r \left(1 + \frac{D_b}{D_c} \cos \beta\right) \quad (2)$$

Ball:

$$f_c = f_B = \frac{D_c}{D_b} f_r \left(1 - \frac{D_b^2}{D_c^2} \cos^2 \beta\right) \quad (3)$$

Cage:

$$f_c = f_{CA} = \frac{f_r}{2}\left(1 - \frac{D_b}{D_c} \cos(\beta)\right) \quad (4)$$

with f_r is the mechanical rotor frequency given by:

$$f_r = \frac{(1-s)}{p} . f_s \quad (5)$$

where s is the rotor slip and f_s fundamental frequency of the stator currents.

III. ANALYSIS BASED ON MCSA-FFT

The spectral stator current under REB faults contains some additional harmonic components given as follows:

$$f^{\pm}_{charact-OR,IR,cage,ball} = \left| \nu f_s \pm k f_{OR,IR,cage,ball} \right| \quad (6)$$

with, $f_{OR,IR,cage,ball} = f_c$ the characteristic frequencies of vibration signal spectrum, ν the order of the stator time harmonics (ν=1,3,5, etc.) and k an integer.

According to [19] and for REBs which has a number of balls between 6 and 12; the characteristic frequencies of the vibration signal can be approximated by:

$$f_{OR} = 0.4 N_b \times k \times f_r \quad (7)$$

$$f_{IR} = 0.6 N_b \times k \times f_r \quad (8)$$

In this study, the frequency analysis is based considering the equations 7 and 8. As the IM is under IR fault we can write:

$$f^{\pm}_{charact-IR-\nu,k} = \left| \nu f_s \pm k f_{IR} \right| \quad (9)$$

It's known that the variation of the slip value depends on the load value. In experimental tests, it is applied a nominal resistant torque giving s = 3.66%. In this case for f_s=50Hz, the f_r value is 48.167Hz. Some specific frequencies in the vibration and stator current spectrum created by inner raceway fault are summarized in Table 1. It gives us an overview of the multitude of harmonics created by the fault.

TABLE I. SUMMARY OF SOME CHARACTERISTIC HARMONICS UNDER IRF (s=0.0366)

Formulas of Characteristic Frequencies in the Vibration Spectrum	*Theoretical values (Hz)*	*Formulas of Characteristic Frequencies in the Stator Current Spectrum*	*Theoretical values (Hz)*
$1\times f_{IR}$	*260.1018*	$\lvert f_s + f_{IR}\rvert$	*310.1018*
$2\times f_{IR}$	*520.2036*	$\lvert f_s - f_{IR}\rvert$	*210.1018*
$3\times f_{IR}$	*780.3054*	$\lvert f_s + 2f_{IR}\rvert$	*570.2036*
$4\times f_{IR}$	*1040.4075*	$\lvert f_s - 2f_{IR}\rvert$	*470.2036*
$5\times f_{IR}$	*1600.509*	$\lvert 3f_s - f_{IR}\rvert$	*110.1018*
$6\times f_{IR}$	*1560.6108*	$\lvert 5f_s + f_{IR}\rvert$	*510.1018*
$7\times f_{IR}$	*1820.7112*	$\lvert 5f_s - f_{IR}\rvert$	*10.1018*
$8\times f_{IR}$	*2080.8144*	$\lvert 5f_s - 2f_{IR}\rvert$	*270.2036*

As an inherent mixed rotor eccentricity always exist even in a healthy machine, the specific frequencies characteristic are given as follow:

$$f_{mix-ecc} = \left| f_s \pm k f_r \right| \tag{10}$$

where, k=1,2,3, ...

In addition to these frequencies, we can define the **R**otor **S**lot **H**armonics (*RSHs*) given by:

$$f_{RSHs} = \left[\frac{k.N_{rb}(1-s)}{p} \pm \nu \right] . f_s \tag{11}$$

where k is an integer. We can also define the saturation frequencies (f_{sat}) expressed as follow [21]:

$$f_{sat} = 3kf_s \tag{12}$$

where k is an odd number.

Equations (1-12) and Table I give us an overview of the specific harmonics created by the fault. Normally, the additional frequencies caused by the IRF also appear in the current spectrum of the stator as can be seen in Fig. 4b, 4d, Fig. 5b, and 5d. In spectrum of measured stator current, it is found some characteristic frequencies of IRF with low amplitude: 10Hz, 110.3Hz, 210.1Hz, 270.4Hz, etc. These frequencies verify (9).

As the mixed eccentricity frequency exists in the stator current spectrum even in healthy IM; the components at f_s+f_r and f_s+3f_r frequency appears in Fig. 4a and 4c (98.3Hz respectively 194.9Hz).

In addition to current harmonics shown in Fig. 4, it is presented in Fig. 5 the Principal Slot Harmonics (PSHs). Figure 5b shows the frequency band 250-550Hz where it is found $5f_s$-$2f_{IR}$ harmonic and Fig. 5d the frequency band 1000-1600Hz. Figures 5a and 5c show only frequencies that are in correspondence with the healthy state of IM. Lower PSH (L-PSH) and Upper PSH (U-PSH) have the values 1195Hz and 1395Hz successively. It's clear that around L-PSH and U-PSH the additional frequencies for IRF do not appear. In presented figures the blue ones correspond to the healthy state of IM and the red ones to the IRF.

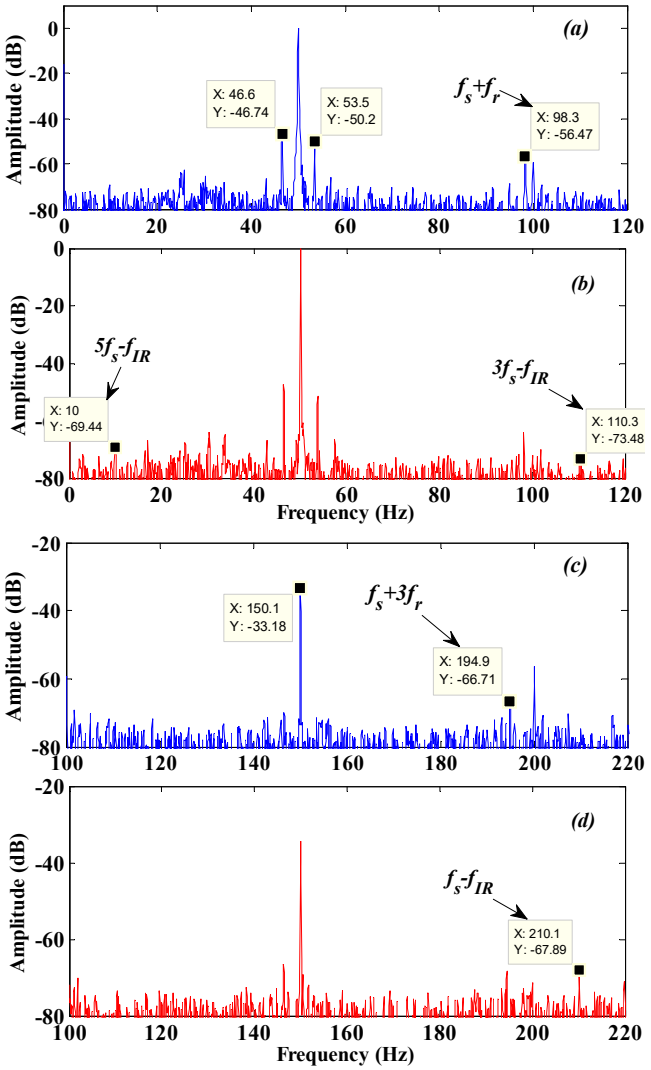

Fig. 4. Stator current spectrum in healthy case (a,c) and IRF case (b, d) for 0-120Hz and 100-220Hz.

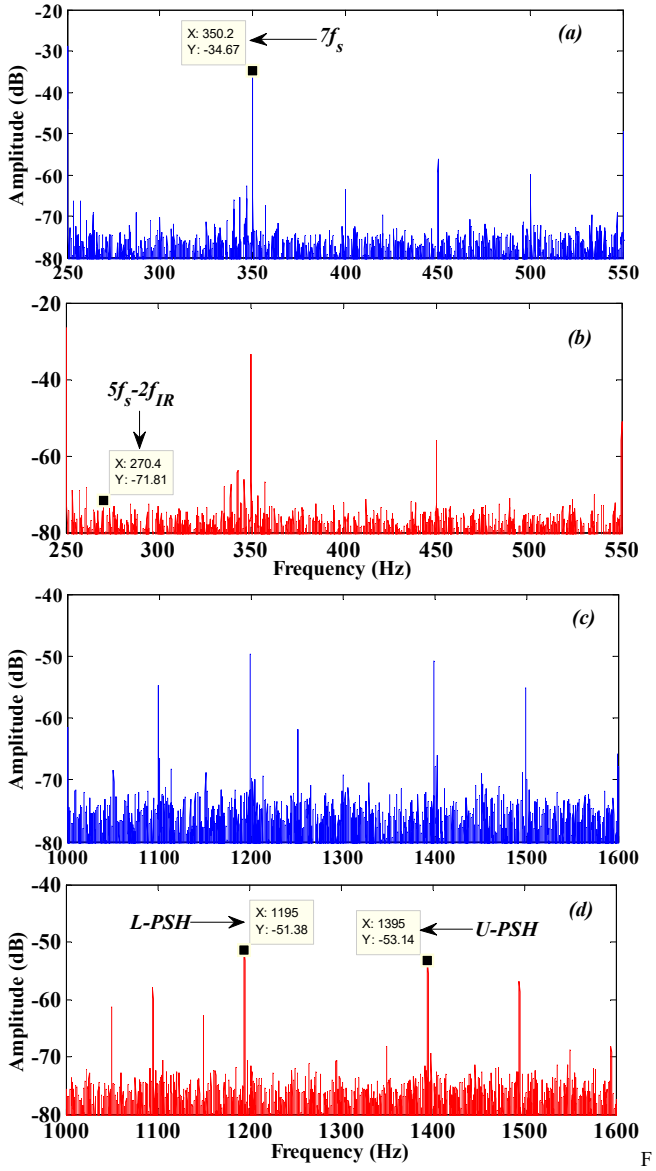

Fig. 5. Stator current spectrum in healthy case (a,c) and IRF case (b, d) for 250-550Hz and1000-1600Hz.

The stator current spectra above show the difference between the healthy and faulty state of IM under IRF. We can notice that the IRF frequencies appear in the stator current spectrum with low amplitude. Here, a sideband frequency is not find around the PSHs (L-PSH and U-PSH) as in the case of broken rotor bar faults. This shows that the PSHs are not affected by the IRF.

The amplitude evolution of the PSHs in case of IRF fault is presented in Table II. We can observe a lower amplitude variation of the PSHs between the healthy and faulty state.

TABLE II. AMPLITUDE EVOLUTION OF PSHS VALUES

PSHs	*Amp. Healthy IM (dB)*	*Amp. Faulty IM (IRF) (dB)*
L-PSH	*-49.65*	*-51.38*
U-PSH	*-50.81*	*-53.14*

IV. ANALYSIS BASED ON MVSA-FFT

This section presents the results obtained by analysing the spectrum of the vibratory signal measured on IM. The measurements are carried out under the same conditions as those used for MCSA at full load (s=0.0366).

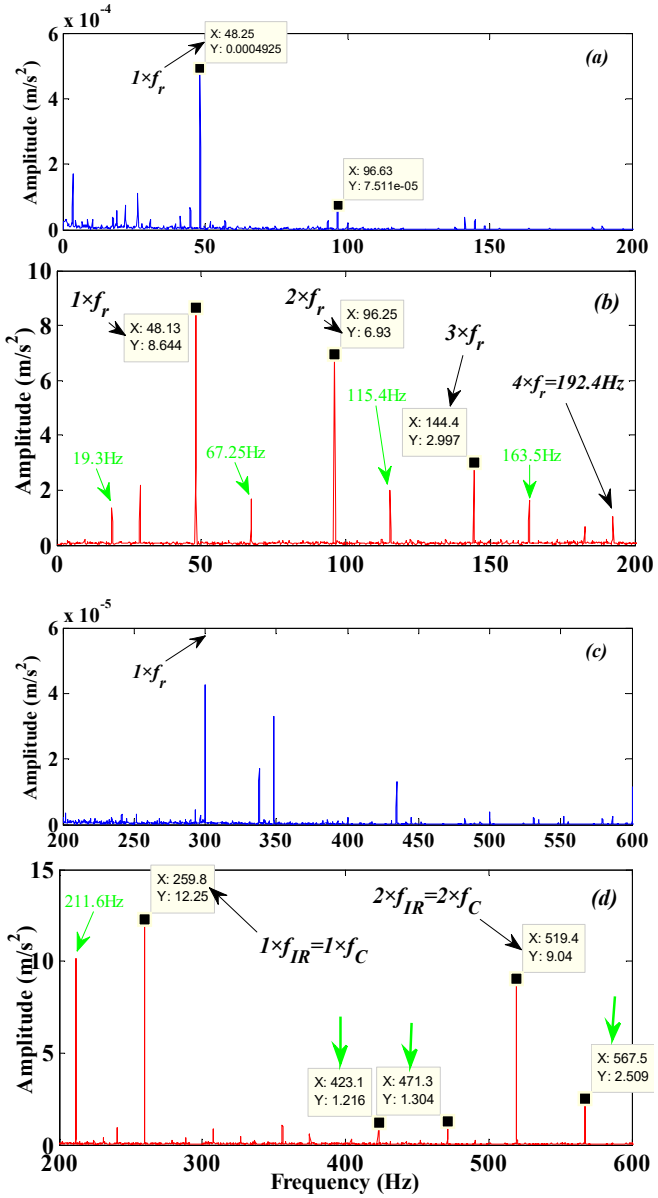

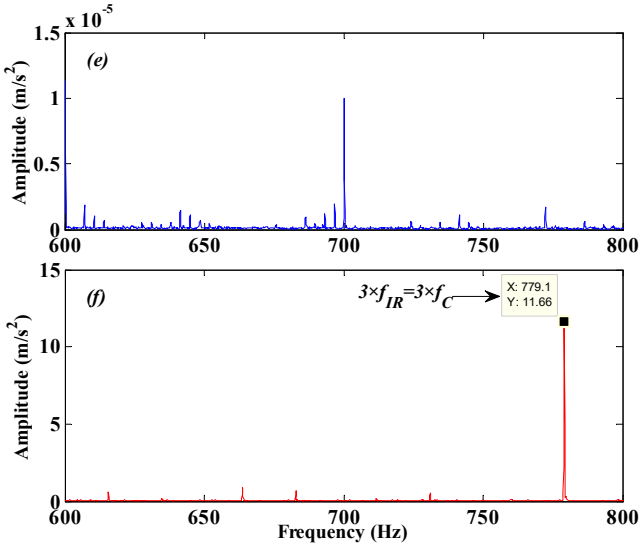

Fig. 6. Spectrum of vibration signal in healthy case (a, c, e) and IRF case (b, d, f) for 0-200 Hz, 200-600Hz, and 600-800Hz.

The comparative spectrum between the healthy state (blue color) and faulty state (red color) presented in Figs. 6-a-b-c-d for the lower frequency bands shows the modification in the amplitude value of harmonics $k\times f_r$. The characteristic frequencies are in accordance with (8) and harmonics presented in Table I.

To achieve good fault detection, it is important to indicate the overlap of f_{IR} with other frequencies. According to the characteristic frequency expression of REB faults (6), it is essential to distinguish between f_{IR}, f_{OR}, and f_{Cage}. The intersection between the characteristic frequencies of ORF, IRF, and cage faults are given as follows [7, 22]:

$$\begin{cases} 3k\times f_{OR} = 2k\times f_{IR} \\ k\times f_{OR} = 9k\times f_C \\ 2k\times f_{OR} = 27k\times f_C \end{cases} \quad (13)$$

with, k=1, 2, 3,…etc.

The relationships between the characteristic frequencies of REB faults show that additional harmonics created by a different type of REB faults may appear in vibration spectrum, what can lead to the confusion in analysis of vibration signal. However the knowledge of the intersection points leads to improve fault detection. For example, in the presented case, the slip value is equal to 0.0366 (i.e. f_r=48.167 Hz).

So, considering (7) and (8) we can found f_{OR}=0.4×9×f_r=173.4012Hz and f_{IR}=0.6×9×f_r=260.1018Hz. It's obtained 3×f_{OR}=520.2036 Hz which is equal to 2×f_{IR}=520.2036 Hz.

Figures 7a and 7b show the characteristic frequencies of the IRF which appear at predicted frequency with great amplitude even for more advanced frequency ranges. The frequencies which characterize this fault are 1×f_{IR}=260.1018 Hz, 2×f_{IR}=520.2036 Hz, 3×f_{IR}=780.3054 Hz, etc.

In addition to characteristic frequencies of the IRF, the Side-Band Frequencies (SBFs) around $k\times f_{IR}$ were sought in the vibratory spectrum. They are identified by a series of harmonics given in [20]:

$$f_{SBF-IR} = k\times f_{IR} \pm k'\times f_r \quad (14)$$

with, k and k' a positive integers.

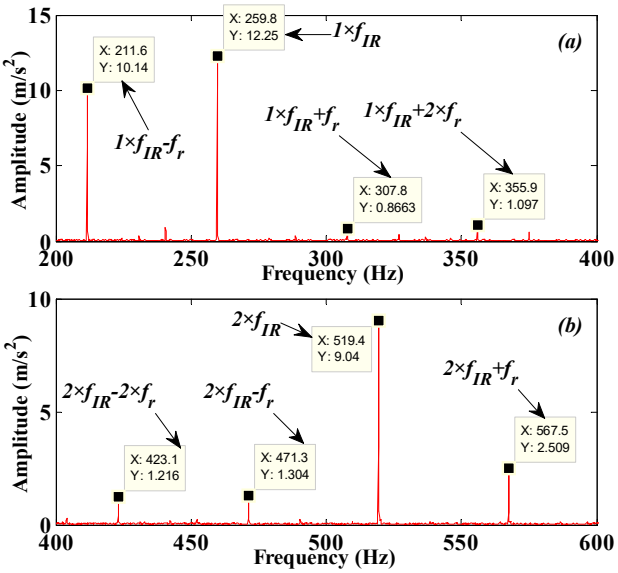

Fig. 7. Appearance of Side-Band Frequencies in vibration signal spectrum under IRF: (a): 200-400 Hz; (b): 400-600Hz.

The SBFs around some characteristic frequencies of IRF were calculated as a function of the rotational speed. Figure 7 shows a zoom around 1×f_{IR} and 2×f_{IR}. We can see here that the SBFs are spaced by f_r.

The presented frequency analysis of the vibration signal shows us the sensibility of this technique in the detection of inner raceway fault. If there is easy access to place a vibration sensor in a "good" frame position of the motor it may be noticed a sensitive variation of characteristic faulty harmonics. However the performances of this technique are limited if the access around the machine is restricted or vibration signal is polluted by external sources (load, shaft misalignment, etc.). In these cases other techniques are necessary.

V. Analysis Based on SFSA-FFT

The **S**tray **F**lux **S**ignature **A**nalysis (SFSA) is an additional investigation technique proposed for analysis of rolling bearing faults [23] based on the stray flux measurement in different positions around the electrical machine. This work uses coil sensors installed in the vicinity of IM frame measuring the radial and axial stray flux. The advantage of these sensors is that they are easy to handle and not require any electronics for implementation of the system. The magnetic flux changes automatically under REB fault, so the electromotive force amplitude varies in the coil sensors. In this study, the FFT is applied to Electro-Motive Force (EMF) waveform and the frequency spectra have been analyzed.

Figure 8 shows the flux spectra in different ranges obtained for IM at full load (s=0.0366) in healthy and IRF cases. It's clear that the blue shape spectrum corresponding to the healthy IM (Fig. 8a) is different from the red shape one (faulty IM 'IRF' Fig. 8b).

The evolution of several amplitudes is visible and detectable in Figs. 8-9 as is the case of sf_s and $3sf_s$ frequency. Associated with mixed eccentricity and air gap variation, their variation is generally a consequence of rotor electrical faults, but as presented in this test, it is also sensitive to rolling bearing failure [24, 25]. The black arrows present new harmonics which appear influenced by IRF in addition of the sf_s and $3sf_s$. Their amplitude evolution is presented in Figs.8-12.

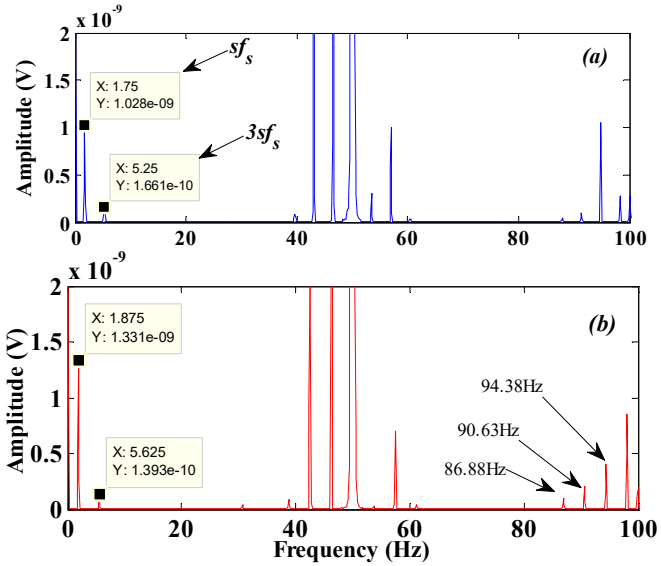

Fig. 8. Flux spectrum: signal in healthy case (a) and IRF case (b) for 0-100Hz.

In practice, the electrical and mechanical faults of the rotor as well as the REB faults have a low influence in the stator currents, however, they lead to an eccentricity of the rotor which will daffect the symmetry of the IM magnetic field.

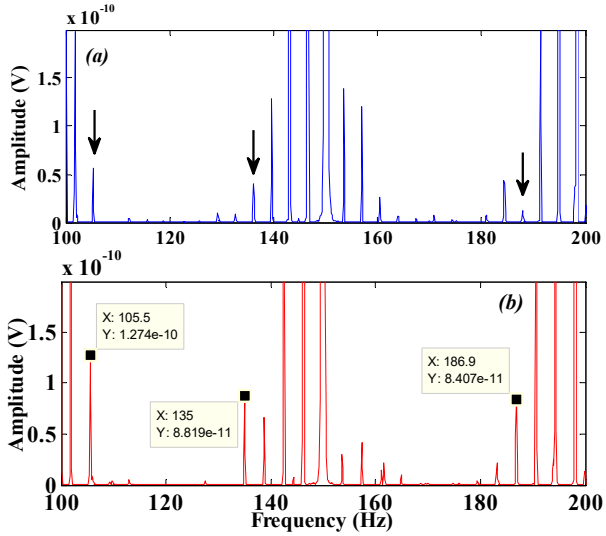

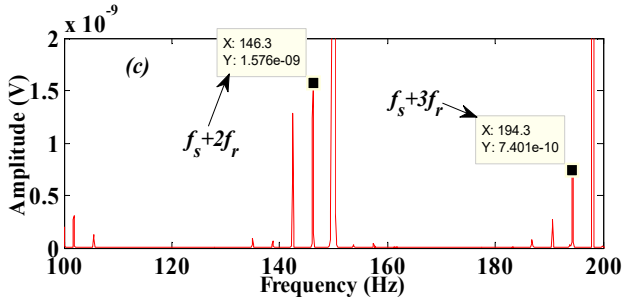

Fig. 9. Flux spectrum: signal in healthy case (a) and IRF case (b) and the zoom of (b) in (c) for 100-200 Hz.

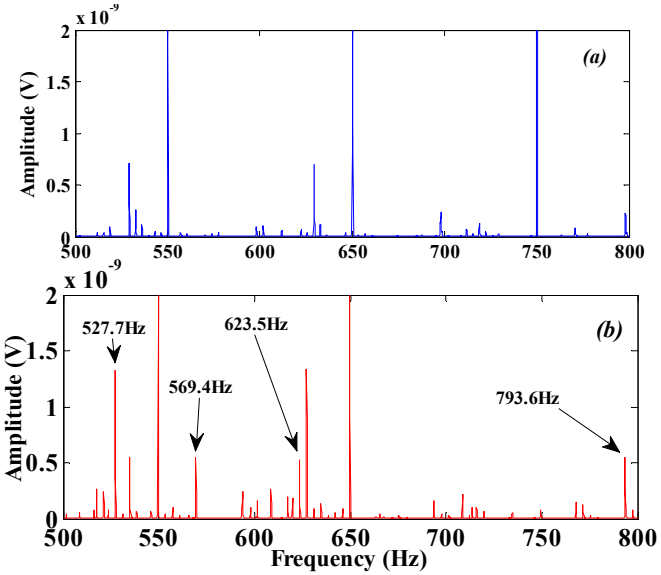

Fig. 10. Flux spectrum: signal in healthy case (a) and IRF case (b) for 500-800 Hz.

According to the above flux spectra measured by the coil sensors, the IRF can be detected in different range frequencies. We can notice here a similarity between the stator current spectrum and the flux spectrum that points towards bearing failures.

The analysis of the flux spectra allows us to find additional harmonics that appear at the same frequency f_s-f_{IR} and f_s+2f_{IR} given by (9) respectively at 209.8H with Amp=5.29e-10V and 569.4Hz with Amp=5.5e-10V. These values presented in Fig. 11 and Fig. 12. confirm the results found in Table 1 (f_{IR}=210.1018Hz and f_s+f_{IR}=570.2036Hz). In addition, other harmonics due to the mixed eccentricity of the rotor clearly appear at f_s+f_r=98.13Hz, $f_s+2\times f_r$=146.3Hz, $f_s+3\times f_r$=194.3Hz, etc. They are in correspondence with (10).

It is important to note that these additional frequencies are the same than these that have been detected in the stator current spectrum. This confirms the relationship between current and flux when one is the image of the other.

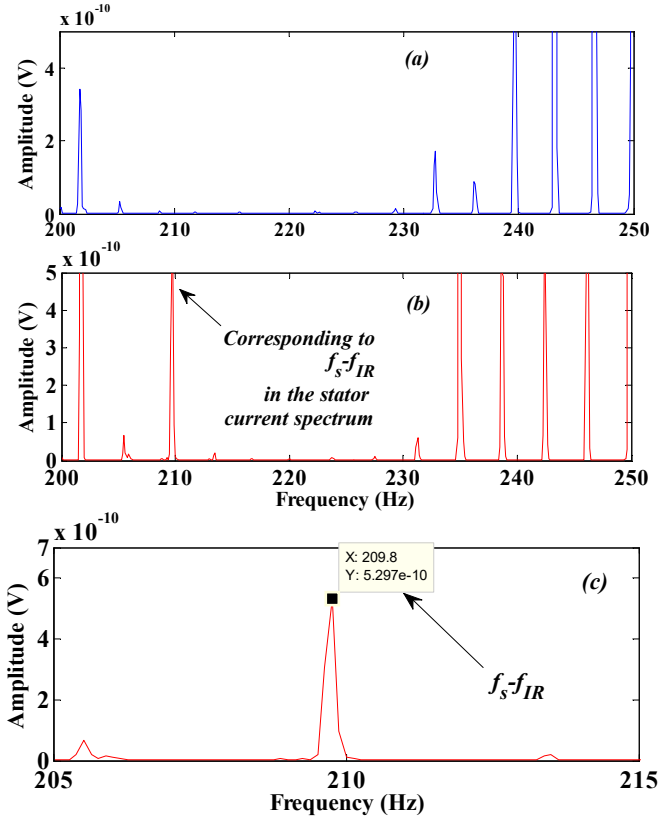

Fig. 11. Flux spectrum; (a): Healthy IM, (b): IRF, (c): Zoom around 210Hz.

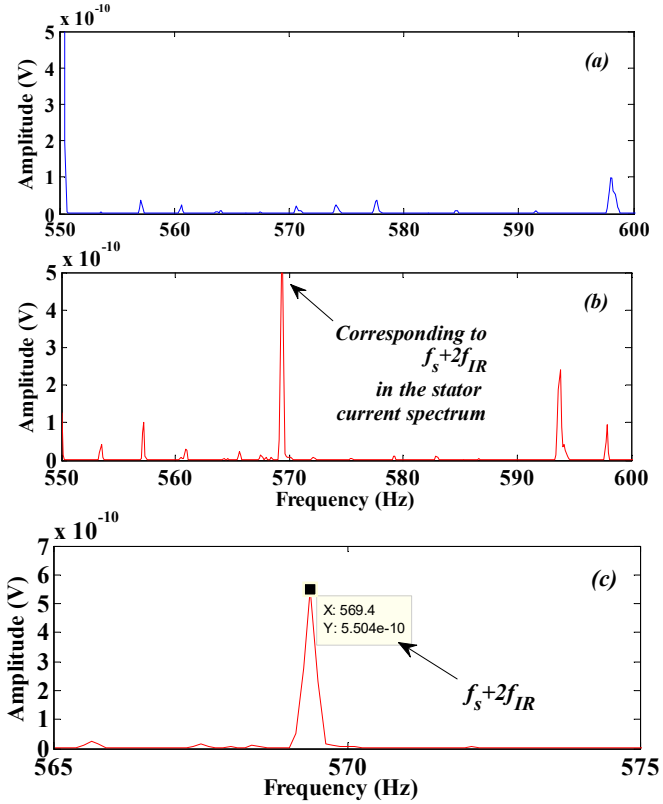

Fig. 12. Flux spectrum; (a): Healthy IM, (b): IRF, (c): Zoom around 570Hz.

We can indicate here the overlap between the frequency sf_s and the frequency f_s-f_r under the pole of the IM which is equal to 1 (p=1) when sf_s=f_s-f_r. The amplitude evolutions of some frequencies of f_s+k×f_r is presented in Table III.

Finally the analysis based on SFSA-FFT shown the sensibility of this technique in the detection of the IRF. This fault changes the current and vibration spectrum but also the stray flux in IM because these three signals are always related together. Figs.8-12 bring to the light the amplitude variation of specific flux harmonics linked at the current and vibration variation but also the appearance of some new harmonics that requires more experimental tests before to be declared as specific IRF signatures.

TABLE III. AMPLITUDE EVOLUTION OF MIXED ECCENTRICITY HARMONICS

f_s±k×f_r	*Amp. Healthy IM (V)*	*Amp. Faulty IM (IRF) (V)*
f_s+f_r	$2.728\times^{-10}$	$8.547\times^{-10}$
f_s+2×f_r	$5.271\times^{-9}$	$1.576\times^{-9}$
f_s+3×f_r	$1.317\times^{-9}$	$7.401\times^{-10}$

VI. CONCLUSION

This paper has presented a comparative study in the application of three diagnosis techniques to detect the Rolling Element Bearingfaults (REB). The MCSA-FFT, MVSA-FFT, and Stray Flux Signature Analysis (SFSA-FFT) are applied to detect the presence of the Inner Raceway Fault (IRF) in Induction Motor.

In summary, the MCS- FFT analysis did not reveal any significant amplitude variation of mixed eccentricity or specific IRF frequencies in the stator current spectrum.

The MVSA-FFThas gave good indices in the vibration signal spectrum but the performance of vibration analysis in the practical application can be easily influenced by external sources as load variation, shaft misalignment, etc.

Stray **F**lux **S**ignature **A**nalysis sensitive to REB gave good information on the IRF. This fault modifies the spectrum of current, vibration, and stray flux because these three signals are always linked to each other. It's therefore found in the stray flux; harmonics linked to the current and the vibration but compared to MVSA, this detection technique is insensitive to external vibrations of the motor. Under these conditions, the use of SFSA-FFT in combination with at least one of the conventional techniques can be an advantageous method for increasing the reliability of the diagnosis.

We also notice here the appearance of other new harmonics, the new challenge is to analyse the limits of their applications.

REFERENCES

[1] O.V. Thorsen, M. Dalva, "A survey of faults on induction motors in offshore oil industry, petrochemical industry, gas terminals, and oil refineries," *IEEE Trans. Industry App.*, 1995.

[2] S. E. Pandarakone, Y. Mizuno, H. Nakamura, "Distinct fault analysis of induction motor bearing using frequency spectrum determination and support vector machine, "*IEEE Tran. Ind. App.* Vol. 53, pp. 3049-3056, 2016.

[3] S. Yeolekar, G. N. Mulay, B. H. Jagdish. "Outer race bearing fault identification of induction motor based on stator current signature by wavelet transform," IEEE International Conference on Recent Trends in Electronics, Information and Communication Technology (RTEICT), pp. 2011-2015, 2017.

[4] M. Ojaghi, M. Mohammadi, "Unified modeling technique for axially uniform and nonuniform eccentricity faults in three-phase squirrel cage induction motors," *IEEE Trans. Ind Electronics*, vol. 65, pp.5292-5301, 2017.

[5] N. Bessous, A. Chemsa, S. Sbaa, "New vision about the mixed eccentricity fault causes in induction motors and its relationship with the rolling element bearing faults: Analytical model dedicated to the REB faults," IEEE International Conference on Communications and Electrical Engineering (ICCEE), pp. 1-11, 2018.

[6] E. Martínez-Montes, L. Jiménez-Chillarón, J. Gilabert-Marzal, J. Antonino-Daviu, A. Quijano-López, "Evaluation of the detectability of bearing faults at different load levels through the analysis of stator currents," IEEE International Conference on Electrical Machines (ICEM), pp. 1855-1860, 2018.

[7] G. A. Capolino, R. Romary, H. Hénao, R. Pusca, "State of the art on stray flux analysis in faulted electrical machines," IEEE Workshop on Electrical Machines Design, Control and Diagnosis (WEMDCD), vol. 1, pp. 181-187, 2019.

[8] J. Martinez, A. Belahcen, A. Muetze, "Analysis of the vibration magnitude of an induction motor with different numbers of broken bars," *IEEE trans.Ind. App.*, vol. 53, pp. 2711-2720, 2017.

[9] K. N. Gyftakis, P. A. Panagiotou, S. B. Lee, "The role of the mechanical speed frequency on the induction motor fault detection via the stray flux," IEEE 12th International Symposium on Diagnostics for Electrical Machines, Power Electronics and Drives (SDEMPED), pp. 201-207, 2019.

[10] Pastor-Osorio, A. Pedro, J. Antonino-Daviu, A. Quijano-Lopez, "Misalignment and rotor fault severity indicators based on the transient DWT analysis of stray flux signals," IEEE Energy Conversion Congress and Exposition (ECCE), pp. 3867-3871, 2019.

[11] H. Zhu, Z. Yang, X. Sun, D. Wang, X. Chen, "Rotor vibration control of a bearingless induction motor based on unbalanced force feed-forward compensation and current compensation," *IEEE Access 8*, pp. 12988-12998, 2020.

[12] G. Mirzaeva, K. I. Saad, "Advanced diagnosis of rotor faults and eccentricity in induction motors based on internal flux measurement," *IEEE Trans. Ind. App.*, vol. 54, pp. 2981-2991, 2018.

[13] I. Zamudio-Ramirez, J. A. Antonino-Daviu, R. A. Osornio-Rios, R. J. Romero-Troncoso, H. Razik, "Detection of winding asymmetries in wound-rotor induction motors via transient analysis of the external magnetic field," *IEEE Trans. Ind. Elect*. 2019.

[14] K. N. Gyftakis, P. A. Panagiotou, S. B. Lee, "The role of the mechanical speed frequency on the induction motor fault detection via the stray flux," IEEE 12th International Symposium on Diagnostics for Electrical Machines, Power Electronics and Drives (SDEMPED), pp. 201-207, 2019.

[15] N. Bessous, S. E. Zouzou, S. Sbaa, A. Khelil, "New vision about the overlap frequencies in the MCSA-FFT technique to diagnose the eccentricity fault in the induction motors," IEEE Conference in Electrical Engineering-Boumerdes (ICEE-B), pp. 1-6, 2017.

[16] G. Georgoulas, V. Climente-Alarcon, J. A. Antonino-Daviu, P. Ioannis Tsoumas, D. C. Stylios, A. Arkkio, G. Nikolakopoulos, "The use of a multilabel classification framework for the detection of broken bars and mixed eccentricity faults based on the start-up transient," *IEEE Trans. Ind. Informatics*, vol. 13, pp. 625-634, 2016.

[17] I. Yilmaz Onel, M. E.H. Benbouzid, " Induction Motor Bearing Failure Detection and Diagnosis: Park and Concordia Transform Approaches Comparative Study" *IEEE/ASME Transactions on Mechatronics,* vol. 13, pp. 257-262, 2008.

[18] M. Iorgulescu and R. Beloiu, "Study of DC motor diagnosis based on the vibration spectrum and current analysis," *IEEE International Conference on Applied and Theoretical Electricity (ICATE)*, Craiova, 2012, pp. 1-4, 2012

[19] R. R. Schoen, T. G. Habetler, F. Kamran and R. G. Bartheld, "Motor bearing damage detection using stator current monitoring," *IEEE Trans. Ind. App.*, vol. 31, pp. 1274-1279, 1995.

[20] E. Martínez-Montes, L. Jiménez-Chillarón, J. Gilabert-Marzal, J. Antonino-Daviu, A. Quijano-López, "Evaluation of the detectability of bearing faults at different load levels through the analysis of stator currents," IEEE International Conference on Electrical Machines (ICEM), pp. 1855-1860, 2018.

[21] N. Bessous, S. Sbaa, A. Toumi, "A detailed study of the spectral content in the stator current of asynchronous machines under broken rotor bar faults using MCSA technique," IEEE International Conference on Control Engineering & Information Technology (CEIT), pp. 1-8, 2018.

[22] N. Bessous, S. Sbaa, R. Bousseksou, A. Allag, "Detailed Study of Rolling Bearing Element Faults in Rotating Electrical Machines using MVSA Technique," *Majlesi Journal of Electrical Engineering*, pp. 75-82, 2019

[23] L. Frosini, M. Minervini, L. Ciceri, A. Albini, "Multiple faults detection in low voltage inverter-fed induction motors," in Proceedings of 2019 SDEMPED, 27-30 Aug. 2019

[24] L. Frosini, C. Harlisca, L. Szabó, "Induction Machine Bearing Fault Detection by Means of Statistical Processing of the Stray Flux Measurement," *IEEE Trans. on Industrial Electronics*, vol.62, n°3, March 2015, pp. 1846-1854.

[25] S. Zhang,B. Wang, M. Kanemaru, C. Lin,D. Liu, K. H. Teo,T. G. Habetler"Quantification of Rolling- Element Bearing Fault Severity of Induction Machines," 2019 IEEE International Electric Machines & Drives Conference (IEMDC), San Diego, CA, USA, 2019, pp. 44-50, 2019